A Bayesian ranking statistic to find high-mass black holes in LIGO–Virgo data

The detection of intermediate-mass black holes ($10^2 - 10^6$ M$_\odot$) will shed light on the formation of supermassive black holes and thus galaxy formation. Although LIGO is sensitive to the merger of binary black holes with total masses up to 400 M$_\odot$, only 4 of their 50 detections have a total mass > 100 M$_\odot$ with $>95\%$ credibility. A possible explanation for the absence of intermediate-mass events may be their misclassification as short-duration instrumental noise transients. Short-duration instrumental transients mimic the short-duration gravitational-wave signals from intermediate-mass binary black hole mergers. [ET: I think the preceding text is misleading. We make it sound like we expect a uniform distribution of total mass, and so it's a surprising that we don't see IMBH. However, in reality, it is theoretically challenging to make IMBH. You need an exceptionally massive progenitor star to avoid pair instability supernova. Or, maybe you can make IMBH from hierarchical mergers or accretion. No one expects them to be common, but they are interesting because of their connection to supermassive black holes. I suggest rewriting the preceding text to explain how IMBH might form and why they are interesting to look for.] Here we demonstrate a ranking statistic utilising Bayesian inference for the detection of high-mass binary black hole mergers (with a total mass > 55 M$_\odot$). [ET: Claims of beating matched filtering not yet borne out.] We apply this technique on the high-mass triggers during LIGO's second observing run to search for previously unresolved gravitational-wave signals from high-mass binary black holes. Our analysis does not discover new gravitational-wave events. However, we find support for some previously identified borderline detections. [ET: Don't oversell Bayesian measure since our method is only semi-Bayesian.]

I. INTRODUCTION

Since the 1970s, there has been a steady accumulation of evidence for stellar mass (M$_{\rm BH} < 10^2$ M$_\odot$) and supermassive black holes (M$_{\rm BH} > 10^5$ M$_\odot$) [1–7]. However, there is a deficiency of observational evidence for black holes in the intermediate-mass range $10^2 - 10^5$ M$_\odot$. Astronomers have detected a handful of intermediate-masses candidates using reverberation mapping, taking direct kinematic measurements, applying M-σ and M-L relations, and also studying X-ray luminosity and spectra [8–13]. However, these observations are highly uncertain and can be attributed to sources without intermediate-mass black holes [? ?]. In the last few years, astronomers have found definitive evidence for two intermediate-mass black holes, (i) the 142^{+28}_{-16} M$_\odot$ remnant observed from the gravitational wave event GW190521 [14], and the $5.5^{+1.7}_{-0.9} \times 10^4$ M$_\odot$ black hole identified from gravitational lensing in the light curve of GRB950830 [15]. The concrete discovery of more intermediate-mass black holes will bridge the observational gap and illuminate our understanding of galaxy and supermassive black hole formation. Additionally, a catalog of observed intermediate-mass black holes can act as probes to their formation environments, such as in the accretion disks of active galactic nuclei [], the centers of dense stellar clusters [], and even Population-III stars [].

Gravitational waves from compact binaries coalesces (CBCs) are clean channels to measure BH masses. Mergers involving either a binary system with at least one intermediate-mass component, or a system whose merger results in an intermediate-mass remnant will have large initial total masses M$_T$. As a binary's M$_T$ is associated with its merger frequency, $f \sim {\rm M}_T^{-1}$, systems with large M$_T$ have very low merger frequencies $f < 100$ Hz. Hence, ground based gravitational wave detectors ($\sim$ 10 − 1000 Hz) are sensitive to the last milliseconds of merging systems with $100{\rm M}_\odot < {\rm M}_T < 400{\rm M}_\odot$ [], while space-based detectors ($\sim$ 0.1 − 10 Hz) can study the full signals of merging systems with $10^4{\rm M}_\odot < {\rm M}_T < 10^7{\rm M}_\odot$ [].

Because of high-total mass systems' short-durations in ground-based gravitational wave data steams, handling data quality is critical to their detection. The low-frequency ranges of ground-based observatories are plagued with incoherent non-stationary terrestrial artefacts, called glitches [16–18]. Some glitches, similar to signals from high total mass mergers, last for a fraction of a second, making them difficult to distinguish from the signals. These glitches that mimic astrophysical signals can severely decrease the confidence in detection of true gravitational-waves from high total mass mergers.

Although a significant fraction of the glitches can be removed by testing them for coherence amongst various ground based detectors and performing matched-filtering, these methods are insufficient to remove all the glitches. One method to account for more glitches while searching for high total mass CBC gravitational-waves is by utilizing the astrophysical Bayesian odds [19–23]. A true Bayesian odds, calculated without using bootstrap techniques, can provide more accurate estimate of significance that does note depend on the search pipeline [21–23]. In this paper, we utilize a Bayesian method, called the Bayesian Coherence Ratio $\rho_{\rm BCR}$ [20], to rank the candidate gravitational-wave signals from high-mass compact binary coalescences (systems with total masses in the range of $55 - 500$ M$_\odot$) in the detector data recorded during O2. Although the $\rho_{\rm BCR}$, utilizing bootstrap techniques, does not provide the true Bayesian odds, it utilizes Bayesian evidences which describe the explicit probability of data under the hypothesis that it contains coherent signals vs incoherent glitches.

[AV: Need to discuss IAS, PyCBC etc here as well]

We find that (a) high-mass events reported in the GWTC-1, including GW170729 (the least significant event in GWTC-1) have high significance; (b) high-mass events detected from the IAS group have differing levels of significance; [ET: differing from what? edit this passage to state more clearly that we find statistical support for some of their candidates, but not for others] and that (c) our ranking statistic does not identify any intermediate-mass black holes, but does identify an unreported stellar-mass binary black hole candidate, 170222 [ET: State statistical significance.].

The remainder of this paper is structured as follows. We outline our methods, including details of our ranking statistic and the retrieval of our candidate events in Section II. We present details on the implementation of our analysis in Section III. Finally, we present our results in Section IV, and discuss these results in the context of the significance of gravitational-wave candidates in Section V.

II. METHOD

The standard framework to identify CBC gravitational-wave signals hidden in data is by quantifying the significance of candidates with null-hypothesis significance testing. In this framework, the candidates' ranking statistic is compared against a background distribution in a frequentist approach. [RS: add a sentence describing what the ranking stats are for the different pipelines (key words: matched filtering, SNR etc...) and add citations!] On the other hand, the standard framework for performing parameter estimation and model selection in gravitational-wave astronomy is Bayesian inference. This work utilizes Bayesian inference to calculate the Bayesian Coherence odds-ratio [20], ρ_{BCR}, of high-mass candidates in LIGO's second observing run. We use the ρ_{BCR} not as an odds-ratio but instead as a ranking statistic, a step toward building a unified Bayesian framework to search for candidates and estimate their parameters.

A. The Bayesian Coherence Ratio

Bayes theorem states that the posterior probability distribution $p(\vec{\theta}|d, \mathcal{H})$ for data d and a vector of parameters $\vec{\theta}$ that describe a model which quantifies a hypothesis $\mathcal{H}$, is given by

$$p(\vec{\theta}|d, \mathcal{H}) = \frac{\mathcal{L}(d|\vec{\theta}, \mathcal{H}) \; \pi(\vec{\theta}|\mathcal{H})}{\mathcal{Z}(d|\mathcal{H})} \; , \tag{1}$$

where $\mathcal{L}(d|\vec{\theta}, \mathcal{H})$ is the likelihood of the data given the parameters $\vec{\theta}$ and the hypothesis, $\pi(\vec{\theta}|\mathcal{H})$ is the prior prob-

ability of the parameters, and finally,

$$\mathcal{Z}(d|\mathcal{H}) = \int_{\vec{\theta}} \mathcal{L}(d|\vec{\theta}, \mathcal{H}) \; \pi(\vec{\theta}|\mathcal{H}) \; d\vec{\theta} \tag{2}$$

is the likelihood after marginalizing over the parameters $\vec{\theta}$. To compare two hypotheses $\mathcal{H}_A$ and $\mathcal{H}_B$ with the Bayes theorem one can calculate an odds-ratio

$$\mathcal{O}_B^A = \frac{\mathcal{Z}^A \; \pi(\vec{\theta}^A)}{\mathcal{Z}^B \; \pi(\vec{\theta}^B)} \; , \tag{3}$$

where $\mathcal{Z}^A$ and $\mathcal{Z}^B$ are the shorthand for the evidences $\mathcal{Z}(d|\mathcal{H}_A)$ and $\mathcal{Z}(d|\mathcal{H}_B)$. The odds-ratio can tell us which of the two hypotheses is more likely. For example, if $\mathcal{O}_B^A >> 1$, then this odds ratio indicates that the $\mathcal{H}_A$ describes the data much better than $\mathcal{H}_B$.

The ρ_{BCR} is a Bayesian odds-ratio like the above, of a coherent signal hypotheses $\mathcal{H}_S$ and an incoherent instrumental feature hypothesis $\mathcal{H}_I$ (the null-hypotheses) for a network of D detectors. $\mathcal{H}_\mathcal{I}$ states that each detector i has either pure stationary Gaussian noise $\mathcal{H}_N$ or Gaussian noise and an incoherent noise transient (glitch). Taking Z^S, Z_i^G and Z_i^N as the Bayesian evidences (marginalised likelihoods, definitions in Appendix **??** for $\mathcal{H}_S$, $\mathcal{H}_N$, and $\mathcal{H}_G$, the ρ_{BCR} is given by

$$\rho_{\mathrm{BCR}} = \frac{\alpha Z^S}{\prod\limits_{i=1}^{D} [\beta Z_i^G + (1 - \beta)Z_i^N]} \; , \tag{4}$$

where α and β are the prior-odds of obtaining a signal or a glitch from a stretch of data. The prior-odds can be defined more explicitly as

- $\alpha = P(\mathcal{H}_S)/P(\mathcal{H}_I)$, the prior-odds for obtaining a coherent signal versus an incoherent instrumental feature.

- $\beta = P(\mathcal{H}_G|\mathcal{H}_I)$, the prior-odds for obtaining a glitch assuming there is an incoherent instrumental feature.

When $\mathcal{H}_S$ and $\mathcal{H}_I$ are precisely described and the correct prior-odds are known, the ρ_{BCR} is a Bayesian odds-ratio. As an odds-ratio, the ρ_{BCR} is the optimal discriminator between coherent signals and incoherent instrumental features. However, as the priors-odds are unknown, it is invalid to use the ρ_{BCR} as an odds-ratio to make an informed decision about whether a candidate is from an astrophysical or terrestrial source. Instead of interpreting the ρ_{BCR} as a Bayesian odds-ratio, it can be used as a ranking statistic. Using the ρ_{BCR} as a ranking statistic we can obtain a frequentist significance of a candidate ρ_{BCR}-value measured against a background ρ_{BCR} distribution.

When using the ρ_{BCR} as a detection statistic, the physical interpretation of the prior-odds is lost. Hence, the

prior-odds are empirically tuned to maximise the separation between the ρ_{BCR} distribution of the background (expected to favour the $\mathcal{H}_I$ hypothesis) and the ρ_{BCR} distribution of artificially manufactured simulated signals (expected to favour the $\mathcal{H}_S$ hypothesis). Increasing the separation between the two distributions can improve ability of the ρ_{BCR} to discriminate candidate events as coherent signals or incoherent instrumental features. The tuning process is described in detail in Appendix B.

B. Calculating the Significance of Candidates

Candidate ρ_{BCR}-values are either statistically insignificant compared to the background ρ_{BCR} distribution, implying the candidate is more probable to be an incoherent instrumental feature (the $\mathcal{H}_I$ null-hypothesis), or statistically significant to the background distribution, indicating the possible presence of an astrophysical signal (the $\mathcal{H}_S$ hypothesis). A false alarm probability with trial factors, FAP, for the candidate ρ_{BCR}-value can quantify the significance. The FAP is the probability that a candidate originating from a non-astrophysical source can be is falsely identified as a signal.

To calculate the FAP, each candidate ρ_{BCR} is considered a single statistical trail that can occur at a fixed false alarm probability f, where f is the probability of observing a background ρ_{BCR}' greater than or equal to the candidate ρ_{BCR},

$$f = \frac{\text{Count of } \rho_{\mathrm{BCR}}' \le \rho_{\mathrm{BCR}}}{\text{Count of } \rho_{\mathrm{BCR}}'} \ . \tag{5}$$

The false alarm probability with trails FAP that the ρ_{BCR} measurement occurs at least once for N trials ($N > 0$), where N is the number of candidate triggers is

$$\mathrm{FAP} = 1 - (1 - f)^N \ . \tag{6}$$

Finally, the FAP can be used to construct a p_{astro}, the probability that a signal is of astrophysical origin [24–26]

$$p_{\mathrm{astro}} = 1 - \mathrm{FAP} \ . \tag{7}$$

C. Data for Analysis

[AV: Probably need a better section label...] The LIGO Scientific collaboration operates several search pipelines that scan for gravitational-waves from compact binary mergers such as `GstLAL`, `MBTA`, `SPIIR` and `PyCBC` [27]. The output of `PyCBC`'s search is a list of times and their corresponding `PyCBC` ranking statistic ρ_{PC} values. The ρ_{PC} ranking-statistic is akin to the matched-filter signal-to-noise ratio ρ. However, unlike ρ, ρ_{PC} includes candidate signal's intrinsic and extrinsic properties and

other information that feeds into determining if the signal can have astrophysical origins [28]. Whenever a local maximum of $\rho_{\mathrm{PC}} > \rho_{\mathrm{T}}$, where ρ_{T} is some predetermined threshold value, the `PyCBC` search pipeline produces a single-detector *trigger* associated with the detector and time where the apparent signal in the data has its merger [28].

When `PyCBC` observes a trigger between detectors with coincident parameters and a time of arrival difference less than the gravitational-wave travel time between detectors, the trigger is labelled a *candidate event trigger*, a trigger that may be from astrophysical origins [29]. To test the pipeline's sensitivity `PyCBC` also conducts searches for *simulated triggers*, artificial triggers manufactured by injecting signals into the detector data. Finally, to quantify the statistical significance of candidate triggers, `PyCBC` artificially constructs *background triggers* to compare against the candidate events. These background triggers are coherent signal-free events, constructed by applying relative offsets, or time-slides, between the data of different detectors [28]. The background trigger's ρ_{PC} distribution is used to calculate the candidate trigger's significance, using null-hypothesis significance testing, under the assumption that all candidate event triggers are due to noise.

Our work demonstrates that the ρ_{BCR} can be used in the same way as ρ_{PC} to measure candidate triggers' statistical significance. The ρ_{BCR} can be a powerful ranking statistic as it incorporates information of not only all possible binary black hole systems that might have merged to produce the trigger but also the various incoherent glitches that might cause a false-detection.

III. ANALYSIS

A. Acquisition of triggers

Advanced LIGO's second observing run O2 lasted 38 weeks [30]. The software package, `PyCBC` [31], was used by LIGO to process the O2 data in 22 time-frames (approximately 2 weeks for one time-frame) and found several gravitational-wave events and numerous gravitational-wave candidates [28, 29, 32–36]. Some candidate events were vetoed to be glitches, while others were rejected due to their low significance. The data is divided into these time-frames because the detector's sensitivity does not stay constant throughout the eight-month-long observing period.

In addition to finding candidate events, `PyCBC` also identified several million background triggers for each time-frame, by searching background data manufactured by time-sliding data within that time-frame. The background triggers help quantify the candidate events' significance for the respective time-frames. Finally, to test the search's sensitivity, `PyCBC` produced and searched for thousands of simulated signals.

For our study, we filter the background, simulated and

TABLE I. High-mass parameter space (parameters correspond to signals with durations < 454 ms).

	Minimum	Maximum
Component Mass 1 [$M_\odot$]	31.54	491.68
Component Mass 2 [$M_\odot$]	1.32	121.01
Total Mass [$M_\odot$]	56.93	496.72
Chirp Mass [$M_\odot$]	8.00	174.56
Mass Ratio	0.01	0.98

candidate events to include only high-mass events with masses in the ranges of the parameters presented in Table I. A plot of the PyCBC triggers from one time-frame, during April 23 - May 8, 2017, is presented in Fig. 1. This figure also depicts the gravitational-wave templates used during the search through this time-frame of data.

B. Calculating the BCR for triggers

[AV: Sat 13th: Just realised that some parts of this dont make sense without the material present in Apdx A]... To evaluate Z^S, Z_i^G and Z_i^N and calculate the ρ_{BCR} Eq. 4 for triggers, we carry out Bayesian inference with BILBY [37, 38], employing DYNESTY [39] as our nested sampler. Nested sampling, an algorithm introduced by Skilling [40, 41], provides an estimate of the true Bayesian evidence and is often utilized for parameter estimation within the LIGO collaboration [37, 42, 43].

The most computationally intensive step during Bayesian inference is evaluating the likelihood $\mathcal{L}(d_i|\mu(\vec{\theta}))$. To accelerate our analysis, we use a likelihood that explicitly marginalizes over coalescence time, phase at coalescence, and luminosity distance (Eq. 80 from Thrane and Talbot [44]). While this marginalized likelihood reduces the run time without introducing errors to our evidence evaluation, it does not generates samples for the marginalized parameters. However, these parameter samples can be calculated as a post-processing step [44].

We set the priors $\pi(\vec{\theta}|\mathcal{H}_S)$ and $\pi(\vec{\theta}|\mathcal{H}_G)$ to be identical. These priors restrict signals with mass parameters in the ranges presented in Table I. The spins are aligned over a uniform range for the dimensionless spin magnitude from $[0,1]$. The luminosity distance prior assigns probability uniformly in comoving volume, with an upper cutoff of 5 Gpc. The full list of the priors, along with their shapes, limits and boundary conditions are documented in Table II.

The waveform template we utilize is IMRPHE-NOMPV2, a phenomenological waveform template constructed in the frequency domain that models the inspiral, merger, and ring-down (IMR) of a compact binary coalescence [46]. Although there exist gravitational-wave templates such as SEOBNRV4PHM [47] which incorporate more physics, such as information on higher-order modes, we use IMRPHENOMPV2 as it is computationally inexpensive compared to others.

We take 31 neighboring, off-source, non-overlapping,

TABLE II. Prior settings for the parameters used during our parameter estimation. The definitions of the parameters are documented in Romero-Shaw *et al.* [45] Table E1.

Parameter	Shape	Limits
$\mathcal{M}/M_\odot$	Uniform	7–180
q	Uniform	0.1–1
$M/M_\odot$	Constraint	50–500
d_L/Mpc	Comoving	100–5000
a_1, a_2	Uniform	0–1
θ_{JN}	Sinusoidal	0–π
ψ	Uniform	0–π
ϕ	Uniform	0–2π
ra	Uniform	0–2π
dec	Cosine	0–2π

4-second segments of time-series data before the analysis data segment d_i to generate the PSD. We use off-source to avoid the inclusion of a signal in the PSD calculation. A Tukey window with 0.2-second roll-offs is applied to each data segment to suppress spectral leakage after which the segments are fast-Fourier transformed and median-averaged to create a PSD [48]. Like other PSD estimation methods, this method adds statistical uncertainties to the PSD [49, 50]. To marginalize over the statistical uncertainty, we use the median-likelihood presented by Talbot and Thrane [49] as a post-processing step. [AV: Greg would like me to discuss the effect of the PSD marginalization in more detail]

We take 31 neighboring off-source non-overlapping 4-second segments of time-series data before the analysis data segment d_i to generate the PSD. A Tukey window with a 0.2-second roll-off is applied to each data segment to suppress spectral leakage. After this the segments are fast-Fourier transformed and median-averaged to create a PSD [48]. Like other PSD estimation methods, this method adds statistical uncertainties to the PSD [49–51]. To marginalize over the statistical uncertainty, we use the median-likelihood presented by Talbot and Thrane [49] as a post-processing step. We find that this post-processing step improves the search efficiency by $x\%$ the details of this calculation are presented in the Appendix C.

Finally, we neglect detector calibration uncertainty and acquire data from from the gravitational-wave Open Science Center [30]. The data we use is the publicly accessible O2 strain data from the Hanford and Livingston detectors, recorded while the detectors are in "Science Mode". We obtain the data using GWPY [52].

C. Assigning p_{astro} to candidate events

After the calculating the ρ_{BCR} for the entire set of high-mass background and simulated triggers, we calculate probability distributions $p_b(\rho_{\mathrm{BCR}})$ and $p_s(\rho_{\mathrm{BCR}})$ for each 2-week time-frame of O2 data. These distributions are used to 'tune' prior-odd α and β values.

Using the tuned prior odds the ρ_{BCR} for the candidate
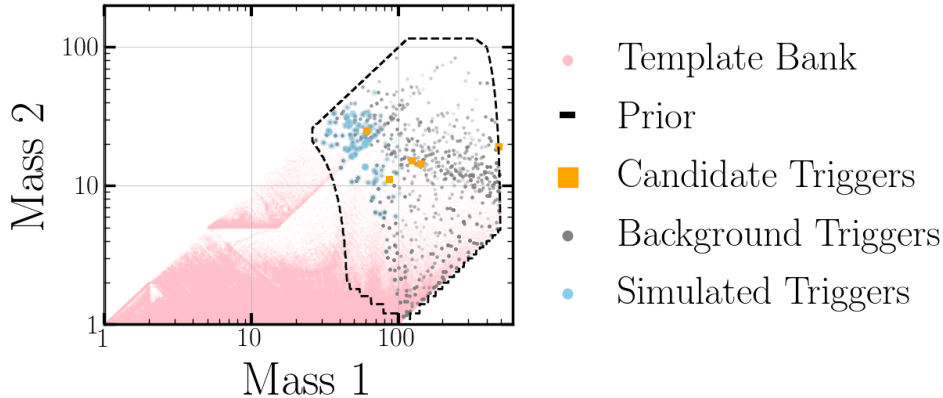
FIG. 1. The template bank (pink) used by PyCBC to search a section of O2 data from April 23 - May 8, 2017. Our search is constrained to the high-mass parameter space enclosed by the dashed line. The candidate, background and simulated triggers detected in this region of the parameter space during this period are plotted in orange, grey and blue respectively. [AV: Should I remove the 'template bank' and only display the various triggers?]

events can be calculated. Fig. 2 shows the ρ_{BCR} distributions for the background triggers, simulated triggers and candidate events. The bulk of the background and simulated trigger distributions are separate but slightly overlap due to some of the simulated signal's being very faint. The separation suggests that the ρ_{BCR} can successfully distinguish signals from noise or glitches. The vertical lines in Fig. 2 displays the ρ_{BCR} for gravitational-wave candidate events. On comparing the candidate event ρ_{BCR} values with the background distribution, we can estimate p_{astro} values for the candidate events.
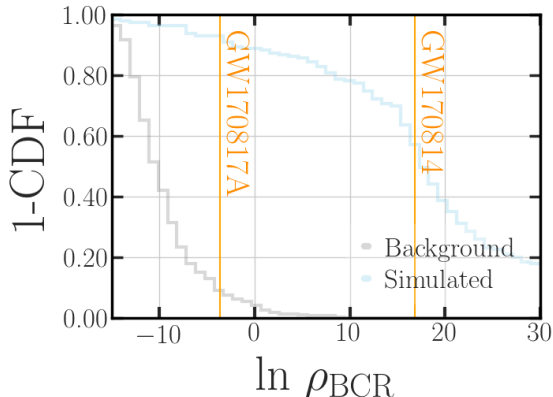

FIG. 2. Histograms represent the survival function (1-CDF) from our high-mass selection of background triggers (grey) and simulated signals (blue) triggers obtained from PyCBC's search of data from August 13 - 21, 2017. Vertical lines mark the ln ρ_{BCR} of IAS's GW170817A and GWTC-1's GW170814.

IV. RESULTS

We analyse the $60,996$ background, $5,146$ simulated, and 25 candidate triggers reported by PyCBC's search on the data from LIGO's second observing run, restricting our analysis to the triggers that fall within our mass-space as described in Section II. We also analyse events and candidate events reported by GWTC-1 and the IAS group (note: some of these were identified as candidates by the PyCBC search). In Table III, we summarise the $p_{\mathrm{astro}}^{\mathrm{BCR}}$, along with the p_{astro} of other pipelines for comparison. Although the various pipeline p_{astro} are not mathematically equivalent, by comparing pipeline p_{astro} values for a given candidate, we can compare how significant each pipeline deems various candidates. The α and β values utilised for each time-frame are reported in Appendix D.

A. GWTC-1 Events

All the confirmed gravitational-wave events from binary black hole mergers reported in GWTC-1 and within our prior space, (specifically GW170104, GW170608, GW170729, GW170809 and GW170814), have $p_{\mathrm{astro}}^{\mathrm{BCR}}$ greater than 0.9, indicating a high probability of the presence of an astrophysical signal.

In addition to the above confirmed gravitational-wave events from GWTC-1, we have also analysed several candidate events from GWTC-1, most of which have low $p_{\mathrm{astro}}^{\mathrm{BCR}}$. For example, consider the candidate event 170412, assigned a p_{astro} of 0.06 by GstLAL and has a $p_{\mathrm{astro}}^{\mathrm{BCR}}$ of 0.01. This candidate was reported to be excess power caused due noise appearing non-stationary between 60-200 Hz [27]. This candidate acts as an example of how $p_{\mathrm{astro}}^{\mathrm{BCR}}$ may be utilised to eliminate candidates originating

TABLE III. The p_{astro} of gravitational wave events from various detection pipelines, along with the event candidates with $p_{\mathrm{astro}}^{\mathrm{BCR}} > 0.3$. Only the candidates and events within our prior space are displayed. The various pipeline p_{astro} represented in this table, $p_{\mathrm{astro}}^{\mathrm{ext}}$, are from the following pipelines: GstLAL ♥ [27], PyCBC ♠ [27], PyCBC OGC-2 ♣ [53], PyCBC 'single-search' ♦ [54], IAS ★ [55, 56], and Pratten and Vecchio [23]'s significances ▲. The catalogues labelled IAS-1 and IAS-2 correspond to the candidates published in Venumadhav *et al.* [55] and Zackay *et al.* [56].

Event	Catalogue	$p_{\mathrm{astro}}^{\mathrm{BCR}}$	$p_{\mathrm{astro}}^{\mathrm{ext}}$	GPS
GW170104	GWTC-1	0.94	$1.00^{♥}; 1.00^{♠}; 1.0^{▲}$	1167559934.60
GW170121	IAS-1	0.76	$1.00^{♣}; 1.00^{★}; 0.53^{▲}$	1169069152.57
170222	-	0.49	-	1171814474.97
170302	IAS-1	0.63	$0.45^{★}; 0.0^{▲}$	1172487815.48
GW170304	IAS-1	0.83	$0.70^{♣}; 0.99^{★}; 0.03^{▲}$	1172680689.36
GWC170402	IAS-2	0.38	$0.68^{★}; 0.03^{♦}; 0.0^{▲}$	1175205126.57
GW170403	IAS-1	0.33	$0.03^{♣}; 0.56^{★}; 0.27^{▲}$	1175295987.22
GW170425	IAS-1	0.10	$0.21^{♣}; 0.77^{★}; 0.74^{▲}$	1177134830.18
GW170608	GWTC-1	0.95	$0.92^{♥}; 1.00^{♠}; 1.0^{▲}$	1180922492.50
GW170727	IAS-1	0.92	$0.99^{♣}; 0.98^{★}; 0.66^{▲}$	1185152686.02
GW170729	GWTC-1	0.96	$0.98^{♥}; 0.52^{♠}; 1.0^{▲}$	1185389805.30
GW170809	GWTC-1	0.98	$0.99^{♥}; 1.00^{♠}; 1.0^{▲}$	1186302517.75
GW170814	GWTC-1	1.00	$1.00^{♥}; 1.00^{♠}; 1.0^{▲}$	1186741859.53
GW170817A	IAS-2	0.83	$0.86^{★}; 0.36^{♦}; 0.02^{▲}$	1186974182.72

from terrestrial noise sources.

B. IAS Events

Our analysis of the high-mass IAS events and candidates in O2 has resulted in three events with disfavourable $p_{\mathrm{astro}}^{\mathrm{BCR}} < 0.5$ (GWC170402, GW170403, GW170425), and four events and one candidate with $p_{\mathrm{astro}}^{\mathrm{BCR}} \geq 0.5$ (GW170121, 170302, GW170304, GW170727, GW170817A). [RS: suggest an additional sentence comparing the numbers with greater/less than 0.5 to the numbers that IAS find.]

GWC170402, detected by Zackay *et al.* [56], is reported to have a signal that is not described well by waveforms for circular binaries with aligned spins [RS: what does "not well described" mean?]. Hence, we might have received a low $p_{\mathrm{astro}}^{\mathrm{BCR}}$ due to our usage of IMRPHENOMPv2, a waveform that does not account for eccentricity. Additionally, the search conducted by Zackay *et al.* [56] was a single-detector search. Our ranking statistic relies on the signal to appear coherent, even if just faintly coherent, amongst the various detectors to have a high $p_{\mathrm{astro}}^{\mathrm{BCR}}$. The lack of coherence and the non-eccentric waveform may be the leading factors for a low p_{astro}. GW170403 and GW170425 which have $p_{\mathrm{astro}}^{\mathrm{BCR}} < 0.35$ also have low p_{astro} reported by Nitz *et al.* [53], suggesting that these events may have been false alarms.

From the candidates with $p_{\mathrm{astro}}^{\mathrm{BCR}} > 0.5$, GW170727 and 170302 are of particular interest, with $p_{\mathrm{astro}}^{\mathrm{BCR}}$ of 0.92 and 0.63. GW170727 was emitted from a black hole binary system with a source frame total mass ≈ 70 $M_{\odot}$. In addition to the high $p_{\mathrm{astro}}^{\mathrm{BCR}}$ reported by our study, Venumadhav *et al.* [55] and Nitz *et al.* [53] have also reported high p_{astro} values of 0.98 and 0.99, making it a viable gravitational-wave event candidate. Similarly, the submarginal-candidate 170302 reported by [55] with a p_{astro} of 0.45 appears to have a higher significance from our analysis, resulting in a $p_{\mathrm{astro}}^{\mathrm{BCR}}$ of 0.63.

C. New Candidate Events

Although no clear detections are made with the ρ_{BCR}, a marginal-candidate 170222 has been discovered with a $p_{\mathrm{astro}}^{\mathrm{BCR}} \sim 0.5$. This candidate has its similar masses when compared to those of GWTC-1. The remaining coherent trigger candidates all have $p_{\mathrm{astro}}^{\mathrm{BCR}} \ll 0.5$ making them unlikely to originate from astrophysical sources.

[AV: mass and spin estimates, is it a vanilla bbh]

V. CONCLUSION

In this paper, we demonstrate that the Bayesian Coherence Ratio [20] can be used as a ranking statistic to provide a better measure of significance for gravitational-wave candidates by re-analysing the significance of high-mass binary black hole triggers from O2. This method takes a step towards building a unified Bayesian frame-

work that provides a search-pipeline agnostic measure of significance, utilising the same level of physical information incorporated during parameter estimation.

We focused our analysis on the high-mass regime as this region of the parameter space is plagued with a high number of short duration terrestrial artefacts that can mimic signals. In addition to the high-mass triggers, we also analyse the high-mass binary black hole events in O2 reported by LIGO [27] and IAS [55, 56]. Using $p_{\mathrm{astro}}^{\mathrm{BCR}}$, we find that the analysed GWTC-1 events have high probabilities of originating from an astrophysical source. We also find that some of the GWTC-1 marginal triggers that have corroborated terrestrial sources (for example candidate 170412) have low $p_{\mathrm{astro}}^{\mathrm{BCR}}$, indicating this method's ability to discriminate between terrestrial artefacts and astrophysical signals. Our analysis on the IAS events has demonstrated that GW17072 is highly likely to originate from an astrophysical source, while GW17040 is not. Finally, we did not identify any new gravitational-wave events, but we did find some a marginal candidate 170222.

Although our analysis targets high-mass triggers, this method can be extended to include the entire body range of LIGO-detectable gravitational-wave sources. Additionally, to further improve the method's infrastructure, we can use more robust gravitational-wave templates (such as templates that incorporate higher-order modes), and sophisticated glitch models. Future analysis can also incorporate data from all available detectors in a network to increase the sensitivity of $p_{\mathrm{astro}}^{\mathrm{BCR}}$. The BCR can discern better whether a candidate is a coherent astrophysical candidate or an incoherent glitch with data from more detectors.

[AV: as the core of this method is PE, improvements in PE can be adapted into this method]

Appendix A: Bayesian Evidence Evaluation

1. Noise Model

We assume that each detector's noise is Gaussian and stationary over the period being analysed [48]. In practice, we assume that the noise has a mean of zero that the noise variance σ^2 is proportional to the noise power spectral density (PSD) $P(f)$ of the data. Using the $P(f)$, for each data segment d_i in each of the i detectors in a network of D detectors, we can write

$$Z_i^N = \mathcal{N}(d_i) = \frac{1}{2\pi P(f)_i} \exp\left(-\frac{1}{2}\frac{d_i}{P(f)_i}\right), \quad \text{(A1)}$$

where $\mathcal{N}(d_i)$ is a normal distribution with $\mu = 0$ and $\sigma^2 \sim P(f)$.

2. Coherent Signal Model

We model coherent signal using a binary black hole waveform template $\mu(\vec{\theta})$, where the vector $\vec{\theta}$ contains a point in the 15 dimensional space describing precessing binary-black hole mergers. For the signal to be coherent, $\vec{\theta}$ must be consistent in each 4-second data segment d_i for a network of D detectors, Hence, the coherent signal evidence is calculated as

$$Z^S = \int\limits_{\vec{\theta}} \prod_{i=1}^{D}\left[\mathcal{L}(d_i|\mu(\vec{\theta}))\right] \pi(\vec{\theta}|\mathcal{H}_S)\,\mathrm{d}\vec{\theta}, \quad \text{(A2)}$$

where $\pi(\vec{\theta}|\mathcal{H}_S)$ is the prior for the parameters in the coherent signal hypothesis, and $\mathcal{L}(d_i|\mu(\vec{\theta}))$ is the likelihood for the coherent signal hypothesis that depends on the gravitational-wave template $\mu(\vec{\theta})$ and its parameters $\vec{\theta}$.

3. Incoherent Glitch Model

Finally, as glitches are challenging to model and poorly understood, we follow Veitch and Vecchio [19] and utilise a surrogate model for glitches: the glitches are modelled using gravitational-wave templates $\mu(\vec{\theta})$ with uncorrelated parameters amongst the different detectors such that $\vec{\theta}_i \neq \vec{\theta}_j$ for two detectors i and j [19]. Modelling glitches with $\mu(\vec{\theta})$ captures the worst case scenario: when glitches are identical to gravitational-wave signals (excluding coherent signals). Thus, we can write Z_i^G as

$$Z_i^G = \int\limits_{\vec{\theta}} \mathcal{L}(d_i|\mu(\vec{\theta}))\,\pi(\vec{\theta}|\mathcal{H}_G)\,\mathrm{d}\vec{\theta}, \quad \text{(A3)}$$

where $\pi(\theta|\mathcal{H}_G)$ is the prior for the parameters in the incoherent glitch hypothesis.

Appendix B: Tuning the prior-odds

After calculating the ρ_{BCR} for a set of background triggers and simulated triggers from as stretch of detector-data (a data chunk), we can compute probability distributions for the background and simulated triggers, $p_b(\rho_{\mathrm{BCR}})$ and $p_s(\rho_{\mathrm{BCR}})$. We expect the background trigger and simulated signal ρ_{BCR} values to favor the incoherent glitch and the coherent signal hypothesis, respectively. Ideally, these distributions representing two unique populations should be distinctly separate and have no overlap in their ρ_{BCR} values. The prior odds parameters α and β from Eq. 4 help separate the two distributions. Altering α translates the ρ_{BCR} probability distributions while adjusting β spreads the distributions. Although Bayesian hyper-parameter estimation can determine the optimal values for α and β, an easier approach is to adjust the parameters for each data chunk's ρ_{BCR} distribution. In this study, we tune α and β to maximally separate the ρ_{BCR} distributions for the background and simulated triggers.

To calculate the separation between $p_b(\rho_{\mathrm{BCR}})$ and $p_s(\rho_{\mathrm{BCR}})$, we use the Kullback–Leibler divergence (KL divergence) D_{KL}, given by

$$D_{KL}(p_b|p_s) = \sum_{x \in \rho_{\mathrm{BCR}}} p_b(x) \log \left(\frac{p_b(x)}{p_a(x)} \right) \; . \qquad \text{(B1)}$$

The $D_{KL} = 0$ when the distributions are identical and increases as the asymmetry between the distributions increases.

We limit our search for the maximum KL-divergence in the α and β ranges of $[10^{-10}, 10^0]$ as values outside this range are nonphysical. We set our values for α and β to those which provide the highest KL-divergence and calculate the ρ_{BCR} for candidate events present in this data chunk. Note that we conduct the analysis in data chunks of a few days rather than an entire data set of a few months as the background may be different at different points of the entire data set.

Appendix C: Marginalizing over PSD statistical uncertainties

To generate the results in Fig. 2, we applied a post-processing step to marginalize the uncertainty in the PSD. In Fig. 3, we show the results if this post-processing step is not applied. Clearly, marginalizing over uncertainty in the PSD yields an improvement in the separation of the noise and signal distributions. Quantitatively, at a threshold $\rho_{\mathrm{BCR}_T} = 0$ the post-processing step results in a reduction in the number of background $\rho_{\mathrm{BCR}} > \rho_{\mathrm{BCR}_T}$ from 60.7% to 25.28% in the August 13 - 21, 2017 time-frame of data. For the entirety of O2 PSD marginalization resulted in a 49.26% improvement in search efficiency.
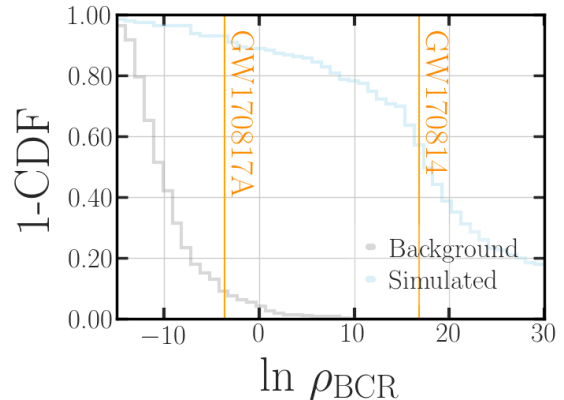

FIG. 3. This plot is analogous to Fig. 2, but without using the post-processing step to marginalize over PSD statistical uncertainties. Without the post-processing step, there is a greater overlap between the background (grey) and foreground (blue) survival functions. For more details about this plot, refer to the caption of Fig. 2.

Appendix D: Tuned prior odds

O2 lasted several months over which the detector's sensitivity varied. Hence, a part of our analysis entailed tuning the prior odds for obtaining a signal and a glitch, α and β, as described in Section II. Table IV presents the signal and glitch prior odds utilised for each time-frame of O2 data.

Tuning the prior odds can dramatically affect the $p_{\mathrm{astro}}^{\mathrm{BCR}}$. For example, consider Table V, which reports tuned $p_{\mathrm{astro}}^{\mathrm{BCR}}$ and un-tuned $p_{\mathrm{astro}}^{\mathrm{BCR}\prime}$ (where $\alpha = 1$ and $\beta = 1$) for various high-mass events and candidates. By tuning the prior odds, the $p_{\mathrm{astro}}^{\mathrm{BCR}}$ for some IAS events (for example, GW170403 and GW170817A) can change by more than 0.5, resulting in the promotion/demotion of a candidate's significance.

[1] B. L. Webster and P. Murdin, Cygnus X-1-a Spectroscopic Binary with a Heavy Companion ?, Nature **235**, 37 (1972).

[2] B. Balick and R. L. Brown, Intense sub-arcsecond structure in the galactic center., ApJ **194**, 265 (1974).

[3] A. M. Ghez, B. L. Klein, M. Morris, and E. E. Becklin, High Proper-Motion Stars in the Vicinity of Sagittarius A*: Evidence for a Supermassive Black Hole at the Center of Our Galaxy, ApJ **509**, 678 (1998), arXiv:astro-ph/9807210 [astro-ph].

[4] R. Genzel, F. Eisenhauer, and S. Gillessen, The Galactic Center massive black hole and nuclear star clus-

TABLE IV. The prior odds used for each time-frame of data from O2. Each time frame commences at the start date and concludes at the following time-frame's start date.

Start Date	α	β
2016-11-15	-	-
2016-11-30	-	-
2016-12-23	1.00E+00	6.25E-01
2017-01-22	-	-
2017-02-03	1.00E-10	2.44E-01
2017-02-12	1.76E-08	5.96E-02
2017-02-20	6.55E-10	2.22E-03
2017-02-28	1.00E-10	5.96E-02
2017-03-10	2.56E-10	3.91E-01
2017-03-18	1.60E-10	1.00E+00
2017-03-27	1.10E-08	5.96E-02
2017-04-04	3.73E-02	2.33E-02
2017-04-14	1.05E-09	2.44E-01
2017-04-23	2.68E-09	1.46E-02
2017-05-08	1.00E+00	2.44E-01
2017-06-18	6.55E-10	3.39E-04
2017-06-30	2.02E-05	5.69E-03
2017-07-15	1.05E-09	9.54E-02
2017-07-27	-	-
2017-08-05	2.12E-04	3.73E-02
2017-08-13	2.68E-09	8.69E-04
2017-08-21	-	-

TABLE V. The BCR p-astro after tuning the prior odds, $p_{\mathrm{astro}}^{\mathrm{BCR}}$, and without tuning the prior odds, $p_{\mathrm{astro}}^{\mathrm{BCR}\prime}$.

Event	Catalogue	$p_{\mathrm{astro}}^{\mathrm{BCR}}$	$p_{\mathrm{astro}}^{\mathrm{BCR}\prime}$
161202	-	0.09	0.41
GW170104	GWTC-1	0.94	0.93
GW170121	IAS-1	0.76	0.72
170206	-	0.11	0.51
170222	-	0.49	0.48
170302	IAS-1	0.63	0.54
GW170304	IAS-1	0.83	0.81
GWC170402	IAS-2	0.38	0.01
GW170403	IAS-1	0.33	0.89
GW170425	IAS-1	0.10	0.22
GW170608	GWTC-1	0.95	0.95
GW170727	IAS-1	0.92	0.96
GW170729	GWTC-1	0.96	0.94
GW170809	GWTC-1	0.98	0.99
GW170814	GWTC-1	1.00	1.00
GW170817A	IAS-2	0.83	0.36

ter, Reviews of Modern Physics **82**, 3121 (2010), arXiv:1006.0064 [astro-ph.GA].

[5] B. P. Abbott, R. Abbott, T. D. Abbott, S. Abraham, and et al., GWTC-1: A Gravitational-Wave Transient Catalog of Compact Binary Mergers Observed by LIGO and Virgo during the First and Second Observing Runs, Physical Review X **9**, 031040 (2019), arXiv:1811.12907 [astro-ph.HE].

[6] Event Horizon Telescope Collaboration, K. Akiyama, A. Alberdi, W. Alef, and et al., First M87 Event Horizon Telescope Results. I. The Shadow of the Supermassive Black Hole, ApJ **875**, L1 (2019), arXiv:1906.11238 [astro-ph.GA].

[7] R. Abbott, T. D. Abbott, S. Abraham, F. Acernese, and et al., GWTC-2: Compact Binary Coalescences Observed by LIGO and Virgo During the First Half of the Third Observing Run, arXiv e-prints , arXiv:2010.14527 (2020), arXiv:2010.14527 [gr-qc].

[8] J. E. Greene and L. C. Ho, Active Galactic Nuclei with Candidate Intermediate-Mass Black Holes, ApJ **610**, 722 (2004), arXiv:astro-ph/0404110 [astro-ph].

[9] A. W. Graham and N. Scott, The M $_{BH}$-L $_{spheroid}$ Relation at High and Low Masses, the Quadratic Growth of Black Holes, and Intermediate-mass Black Hole Candidates, ApJ **764**, 151 (2013), arXiv:1211.3199 [astro-ph.CO].

[10] M. Mezcua, Observational evidence for intermediate-mass black holes, International Journal of Modern Physics D **26**, 1730021 (2017), arXiv:1705.09667 [astro-ph.GA].

[11] F. Koliopanos, Intermediate Mass Black Holes: A Review, in *XII Multifrequency Behaviour of High Energy Cosmic Sources Workshop (MULTIF2017)* (2017) p. 51, arXiv:1801.01095 [astro-ph.GA].

[12] D. Lin, J. Strader, A. J. Romanowsky, J. A. Irwin, O. Godet, D. Barret, N. A. Webb, J. Homan, and R. A. Remillard, Multiwavelength Follow-up of the Hyperluminous Intermediate-mass Black Hole Candidate 3XMM J215022.4-055108, ApJ **892**, L25 (2020), arXiv:2002.04618 [astro-ph.HE].

[13] J. E. Greene, J. Strader, and L. C. Ho, Intermediate-Mass Black Holes, ARA&A **58**, 257 (2020), arXiv:1911.09678 [astro-ph.GA].

[14] R. Abbott, T. D. Abbott, S. Abraham, F. Acernese, and et al., GW190521: A Binary Black Hole Merger with a Total Mass of 150 M$_\odot$, Phys. Rev. Lett. **125**, 101102 (2020), arXiv:2009.01075 [gr-qc].

[15] J. Paynter, R. Webster, and E. Thrane, Evidence for an intermediate-mass black hole from a gravitationally lensed gamma-ray burst, Nature Astronomy 10.1038/s41550-021-01307-1 (2021).

[16] A. H. Nitz, Distinguishing short duration noise transients in LIGO data to improve the PyCBC search for gravitational waves from high mass binary black hole mergers, Classical and Quantum Gravity **35**, 035016 (2018), arXiv:1709.08974 [gr-qc].

[17] J. Powell, Parameter estimation and model selection of gravitational wave signals contaminated by transient detector noise glitches, Classical and Quantum Gravity **35**, 155017 (2018), arXiv:1803.11346 [astro-ph.IM].

[18] M. Cabero, A. Lundgren, A. H. Nitz, T. Dent, D. Barker, E. Goetz, J. S. Kissel, L. K. Nuttall, P. Schale, R. Schofield, and D. Davis, Blip glitches in Advanced LIGO data, Classical and Quantum Gravity **36**, 155010 (2019), arXiv:1901.05093 [physics.ins-det].

[19] J. Veitch and A. Vecchio, Bayesian coherent analysis of in-spiral gravitational wave signals with a detector network, Phys. Rev. D **81**, 062003 (2010), arXiv:0911.3820 [astro-ph.CO].

[20] M. Isi, R. Smith, S. Vitale, T. J. Massinger, J. Kanner, and A. Vajpeyi, Enhancing confidence in the detection of gravitational waves from compact binaries using signal coherence, Phys. Rev. D **98**, 042007 (2018), arXiv:1803.09783 [gr-qc].

[21] G. Ashton, E. Thrane, and R. J. E. Smith, Gravitational wave detection without boot straps: A Bayesian approach, Phys. Rev. D **100**, 123018 (2019), arXiv:1909.11872 [gr-qc].

[22] G. Ashton and E. Thrane, The astrophysical odds of GW151216, MNRAS 10.1093/mnras/staa2332 (2020), arXiv:2006.05039 [astro-ph.HE].

[23] G. Pratten and A. Vecchio, Assessing gravitational-wave binary black hole candidates with Bayesian odds, arXiv e-prints , arXiv:2008.00509 (2020), arXiv:2008.00509 [gr-qc].

[24] W. M. Farr, J. R. Gair, I. Mandel, and C. Cutler, Counting and confusion: Bayesian rate estimation with multiple populations, Phys. Rev. D **91**, 023005 (2015), arXiv:1302.5341 [astro-ph.IM].

[25] S. J. Kapadia, S. Caudill, J. D. E. Creighton, W. M. Farr, G. Mendell, A. Weinstein, K. Cannon, H. Fong, P. Godwin, R. K. L. Lo, R. Magee, D. Meacher, C. Messick, S. R. Mohite, D. Mukherjee, and S. Sachdev, A self-consistent method to estimate the rate of compact binary coalescences with a Poisson mixture model, Classical and Quantum Gravity **37**, 045007 (2020), arXiv:1903.06881 [astro-ph.HE].

[26] S. M. Gaebel, J. Veitch, T. Dent, and W. M. Farr, Digging the population of compact binary mergers out of the noise, MNRAS **484**, 4008 (2019), arXiv:1809.03815 [astro-ph.IM].

[27] B. P. Abbott, R. Abbott, T. D. Abbott, *et al.* (LIGO Scientific Collaboration and Virgo Collaboration), GWTC-1: A Gravitational-Wave Transient Catalog of Compact Binary Mergers Observed by LIGO and Virgo during the First and Second Observing Runs, Phys. Rev. X **9**, 031040 (2019).

[28] G. S. Davies, T. Dent, M. Tápai, I. Harry, C. McIsaac, and A. H. Nitz, Extending the PyCBC search for gravitational waves from compact binary mergers to a global network, Phys. Rev. D **102**, 022004 (2020), arXiv:2002.08291 [astro-ph.HE].

[29] B. Allen, χ^2 time-frequency discriminator for gravitational wave detection, Phys. Rev. D **71**, 062001 (2005), arXiv:gr-qc/0405045 [gr-qc].

[30] The LIGO Scientific Collaboration, the Virgo Collaboration, R. Abbott, T. D. Abbott, S. Abraham, F. Acernese, K. Ackley, C. Adams, R. X. Adhikari, V. B. Adya, and et al., Open data from the first and second observing runs of Advanced LIGO and Advanced Virgo, arXiv e-prints ,

[31] A. Nitz, I. Harry, D. Brown, C. M. Biwer, J. Willis, T. D. Canton, C. Capano, L. Pekowsky, T. Dent, A. R. Williamson, G. S. Davies, S. De, M. Cabero, B. Machenschalk, P. Kumar, S. Reyes, D. Macleod, F. Pannarale, dfinstad, T. Massinger, M. Tápai, L. Singer, S. Khan, S. Fairhurst, S. Kumar, A. Nielsen, shasvath, I. Dorrington, A. Lenon, and H. Gabbard, gwastro/pycbc: PyCBC Release 1.16.4 (2020).

[32] B. Allen, W. G. Anderson, P. R. Brady, D. A. Brown, and J. D. E. Creighton, FINDCHIRP: An algorithm for detection of gravitational waves from inspiraling compact binaries, Phys. Rev. D **85**, 122006 (2012), arXiv:gr-qc/0509116 [gr-qc].

[33] A. H. Nitz, T. Dent, T. Dal Canton, S. Fairhurst, and D. A. Brown, Detecting Binary Compact-object Mergers with Gravitational Waves: Understanding and Improving the Sensitivity of the PyCBC Search, ApJ **849**, 118 (2017), arXiv:1705.01513 [gr-qc].

[34] T. Dal Canton, A. H. Nitz, A. P. Lundgren, A. B. Nielsen, D. A. Brown, T. Dent, I. W. Harry, B. Krishnan, A. J. Miller, K. Wette, K. Wiesner, and J. L. Willis, Implementing a search for aligned-spin neutron star-black hole systems with advanced ground based gravitational wave detectors, Phys. Rev. D **90**, 082004 (2014), arXiv:1405.6731 [gr-qc].

[35] S. A. Usman, A. H. Nitz, I. W. Harry, C. M. Biwer, D. A. Brown, M. Cabero, C. D. Capano, T. Dal Canton, T. Dent, S. Fairhurst, M. S. Kehl, D. Keppel, B. Krishnan, A. Lenon, A. Lundgren, A. B. Nielsen, L. P. Pekowsky, H. P. Pfeiffer, P. R. Saulson, M. West, and J. L. Willis, The PyCBC search for gravitational waves from compact binary coalescence, Classical and Quantum Gravity **33**, 215004 (2016), arXiv:1508.02357 [gr-qc].

[36] A. H. Nitz, T. Dal Canton, D. Davis, and S. Reyes, Rapid detection of gravitational waves from compact binary mergers with PyCBC Live, Phys. Rev. D **98**, 024050 (2018), arXiv:1805.11174 [gr-qc].

[37] G. Ashton, M. Hübner, P. Lasky, and C. Talbot, Bilby: A User-Friendly Bayesian Inference Library (2019).

[38] G. Ashton, I. Romero-Shaw, C. Talbot, C. Hoy, and S. Galaudage, bilby pipe: 1.0.1 (2020).

[39] J. S. Speagle, DYNESTY: a dynamic nested sampling package for estimating Bayesian posteriors and evidences, MNRAS **493**, 3132 (2020), arXiv:1904.02180 [astro-ph.IM].

[40] J. Skilling, Nested Sampling, in *Bayesian Inference and Maximum Entropy Methods in Science and Engineering: 24th International Workshop on Bayesian Inference and Maximum Entropy Methods in Science and Engineering*, American Institute of Physics Conference Series, Vol. 735, edited by R. Fischer, R. Preuss, and U. V. Toussaint (2004) pp. 395–405.

[41] J. Skilling, Nested sampling for general Bayesian computation, Bayesian Analysis **1**, 833 (2006).

[42] G. Ashton, M. Hübner, P. D. Lasky, C. Talbot, K. Ackley, S. Biscoveanu, Q. Chu, A. Divakarla, P. J. Easter, B. Goncharov, F. Hernandez Vivanco, J. Harms, M. E. Lower, G. D. Meadors, D. Melchor, E. Payne, M. D. Pitkin, J. Powell, N. Sarin, R. J. E. Smith, and E. Thrane, BILBY: A User-friendly Bayesian Inference Library for Gravitational-wave Astronomy, ApJS **241**, 27 (2019), arXiv:1811.02042 [astro-ph.IM].

[43] R. J. E. Smith, G. Ashton, A. Vajpeyi, and C. Tal-

bot, Massively parallel Bayesian inference for transient gravitational-wave astronomy, MNRAS **498**, 4492 (2020), arXiv:1909.11873 [gr-qc].

[44] E. Thrane and C. Talbot, An introduction to Bayesian inference in gravitational-wave astronomy: Parameter estimation, model selection, and hierarchical models, PASA **36**, e010 (2019), arXiv:1809.02293 [astro-ph.IM].

[45] I. M. Romero-Shaw, C. Talbot, S. Biscoveanu, V. D'Emilio, G. Ashton, *et al.*, Bayesian inference for compact binary coalescences with BILBY: validation and application to the first LIGO-Virgo gravitational-wave transient catalogue, MNRAS **499**, 3295 (2020), arXiv:2006.00714 [astro-ph.IM].

[46] S. Khan, S. Husa, M. Hannam, F. Ohme, M. Pürrer, X. J. Forteza, and A. Bohé, Frequency-domain gravitational waves from nonprecessing black-hole binaries. II. A phenomenological model for the advanced detector era, Physical Review D **93**, 044007 (2016).

[47] S. Ossokine, A. Buonanno, S. Marsat, R. Cotesta, S. Babak, T. Dietrich, R. Haas, I. Hinder, H. P. Pfeiffer, M. Pürrer, C. J. Woodford, M. Boyle, L. E. Kidder, M. A. Scheel, and B. Szilágyi, Multipolar effective-one-body waveforms for precessing binary black holes: Construction and validation, Phys. Rev. D **102**, 044055 (2020), arXiv:2004.09442 [gr-qc].

[48] B. P. Abbott, R. Abbott, T. D. Abbott, *et al.*, A guide to LIGO-Virgo detector noise and extraction of transient gravitational-wave signals, arXiv e-prints , arXiv:1908.11170 (2019), arXiv:1908.11170 [gr-qc].

[49] C. Talbot and E. Thrane, Gravitational-wave astronomy with an uncertain noise power spectral density, arXiv e-prints , arXiv:2006.05292 (2020), arXiv:2006.05292 [astro-ph.IM].

[50] K. Chatziioannou, C.-J. Haster, T. B. Littenberg, W. M. Farr, S. Ghonge, M. Millhouse, J. A. Clark, and N. Cornish, Noise spectral estimation methods and their impact on gravitational wave measurement of compact binary mergers, Phys. Rev. D **100**, 104004 (2019).

[51] S. Biscoveanu, C.-J. Haster, S. Vitale, and J. Davies, Quantifying the effect of power spectral density uncertainty on gravitational-wave parameter estimation for compact binary sources, Phys. Rev. D **102**, 023008 (2020), arXiv:2004.05149 [astro-ph.HE].

[52] D. Macleod, A. L. Urban, S. Coughlin, T. Massinger, M. Pitkin, paulaltin, J. Areeda, E. Quintero, T. G. Badger, L. Singer, and K. Leinweber, gwpy/gwpy: 1.0.1 (2020).

[53] A. H. Nitz, T. Dent, G. S. Davies, S. Kumar, C. D. Capano, I. Harry, S. Mozzon, L. Nuttall, A. Lundgren, and M. Tápai, 2-OGC: Open Gravitational-wave Catalog of Binary Mergers from Analysis of Public Advanced LIGO and Virgo Data, ApJ **891**, 123 (2020), arXiv:1910.05331 [astro-ph.HE].

[54] A. H. Nitz, T. Dent, G. S. Davies, and I. Harry, A Search for Gravitational Waves from Binary Mergers with a Single Observatory, ApJ **897**, 169 (2020), arXiv:2004.10015 [astro-ph.HE].

[55] T. Venumadhav, B. Zackay, J. Roulet, L. Dai, and M. Zaldarriaga, New Binary Black Hole Mergers in the Second Observing Run of Advanced LIGO and Advanced Virgo, arXiv e-prints , arXiv:1904.07214 (2019), arXiv:1904.07214 [astro-ph.HE].

[56] B. Zackay, L. Dai, T. Venumadhav, J. Roulet, and M. Zaldarriaga, Detecting Gravitational Waves With Disparate Detector Responses: Two New Binary Black Hole Mergers, arXiv e-prints , arXiv:1910.09528 (2019), arXiv:1910.09528 [astro-ph.HE].